S E S 2 0 2 6
Twenty-second International Scientific Conference
SPACE, ECOLOGY, SAFETY
20 – 24 October 2026, Stara Zagora, Bulgaria

PRESERVATION OF EXTREME NO_2 EPISODES UNDER CLOUDY CONDITIONS IN TWO EUROPEAN STAGNATION BASINS: SOFIA AND THE PO VALLEY

Plamen Trenchev, Daniela Avetisyan, Elena Trencheva

Space Research and Technology Institute – Bulgarian Academy of Sciences
e-mail: ptrenchev@space.bas.bg; davetisyan@space.bas.bg; etrencheva@space.bas.bg

Keywords: *TROPOMI NO_2; stagnation basin; temperature inversion; shadow manifold reconstruction; extreme-episode preservation; MNAR missingness*

Abstract: *The most severe winter NO_2 pollution episodes in enclosed basins coincide with temperature inversions and persistent cloud cover, precisely when satellite observations are missing. We examine in parallel two of the most affected European basins, Sofia and Milano in the Po Valley. Their episodes are reconstructed using analogue inference on a reconstructed attractor and benchmarked against Random Forest, climatology, persistence and linear interpolation. In Milano, two successive inversion episodes in autumn 2022 (observed columns of 414 and 405 µmol m^{-2}) are reproduced by the nonlinear method, with MOR_ext reaching 0.915, while Random Forest systematically underestimates every peak. In Sofia, every non-EDM method returns MOR_ext = 0.000 at the per-replicate level under the MCAR mask (ε = 10th percentile, E = 3, q = 0.95). In both basins, the RMSE advantage over Random Forest denied ground-level NO_2 exceeds a factor of four. Spatial-mismatch control stations located across orographic barriers (Plovdiv for Sofia, Genova for Milano) confirm that the reconstructed dynamics are basin-specific rather than regional (Δρ = 0.210 and 0.101). The stronger decoupling at Sofia is consistent with its more enclosed topography. We discuss the implications for exposure assessment during episodes that standard satellite products miss.*

ЗАПАЗВАНЕ НА ЕКСТРЕМНИТЕ ЕПИЗОДИ НА ЗАМЪРСЯВАНЕ С NO_2 ПРИ ОБЛАЧНИ УСЛОВИЯ В ДВА ЕВРОПЕЙСКИ БАСЕЙНА С АТМОСФЕРНА СТАГНАЦИЯ: СОФИЙСКАТА КОТЛОВИНА И ДОЛИНАТА НА РЕКА ПО

Пламен Тренчев, Даниела Аветисян, Елена Тренчева

Институт за космически изследвания и технологии – Българска академия на науките
e-mail: ptrenchev@space.bas.bg; davetisyan@space.bas.bg; etrencheva@space.bas.bg

Ключови думи: *TROPOMI NO_2; басейн на застоя; температурна инверсия; реконструкция на сенчевия манифолд; запазване на екстремни епизоди; липсващи данни в MNAR*

Резюме: *Най-тежките епизоди на замърсяване с NO_2 през зимата в затворените басейни съвпадат с температурни инверсии и продължителна облачност – точно когато липсват сателитни наблюдения. Ние разглеждаме паралелно два от най-засегнатите европейски басейни – София и Милано в долината на река По. Епизодите в тях са реконструирани чрез аналогово заключение въз основа на реконструиран атрактор и са сравнени с методите „Random Forest“, климатология, персистенция и линейна интерполация. В Милано два последователни епизода на температурна инверсия през есента на 2022 г. (наблюдавани колони от 414 и 405 µmol m^{-2}) се възпроизвеждат чрез нелинейния метод, като MOR_ext достига 0,915, докато „Random Forest“ систематично подценява всеки пик. В София всеки метод, различен от EDM, дава MOR_ext = 0,000 на ниво реплика при маска MCAR (ε = 10-ти процентил, E = 3, q = 0,95). И в двата басейна предимството на RMSE спрямо „Random Forest“ при NO_2 на нивото на земната повърхност надвишава четирикратно. Контролните станции с пространствено несъответствие, разположени от двете страни на орографски бариери (Пловдив за София, Генуа за Милано), потвърждават, че реконструираната динамика е специфична за всеки басейн, а не регионална (Δρ = 0,210 и 0,101). По-силното разграничаване в София е в съответствие с по-затворената ѝ топография. Обсъждаме последствията за оценката на експозицията по време на епизоди, които стандартните сателитни продукти пропускат.*

Introduction

Satellite NO_2 observations are missing exactly when they matter most. Cloud and quality screening removes roughly two thirds of TROPOMI pixels over Europe, and the loss is concentrated in winter [1, 2]. The synoptic conditions that produce persistent cloud cover – stagnant high-pressure systems, weak winds, shallow boundary layers – are the same conditions that produce the severe NO_2 accumulation episodes relevant to exposure assessment [3,4]. Missingness is therefore structured rather than incidental: it is Missing Not At Random (MNAR) with respect to the quantity being measured.

The consequence for gap-filling is specific. Kriging, inverse-distance weighting and machine-learning regressors are fitted to minimise a pointwise loss, which drives the predicted distribution toward its conditional mean [5, 6]. Under MNAR missingness the omitted observations lie disproportionately in the upper tail, so the fitted model is trained on a truncated distribution and reproduces a truncated distribution. The reconstructed series is smooth, has low RMSE, and has lost the episodes. The failure is structural rather than a matter of tuning. A predictor that minimises squared error has its optimum at the conditional mean, so variance compression is the correct solution to the objective it was given, not a defect in its implementation. Two consequences follow: no amount of hyperparameter search recovers the tail, and an error metric computed over the full distribution cannot detect that the tail is missing.

Enclosed basins are the limiting case. Orographic confinement suppresses ventilation, so inversion episodes are both more intense and more persistent than in open terrain, and the associated cloud cover is more durable. Two European basins illustrate the problem at comparable severity under different topographic geometries. Sofia sits in a closed depression bounded by Vitosha to the south, the Balkan range to the north and Lyulin to the west, with winter episodes driven by residential solid-fuel combustion superimposed on traffic emissions [7, 8]. The Po Valley is bounded by the Alps and the Apennines and sustains some of the highest NO_2 column densities in Europe during autumn and winter stagnation [9, 10].

This paper treats the basin, not the algorithm, as the unit of analysis. We apply a published nonlinear reconstruction framework [11] to Sofia and Milano in parallel and ask three questions. Does the winter inversion regime occupy a distinct, recoverable region of the reconstructed state space in both basins? Are extreme episodes preserved under reconstruction where conventional baselines compress them? And is the recovered dynamical structure specific to the basin, or merely a regional signal that any nearby station would reproduce? The third question is addressed by a negative control that is, to our knowledge, uncommon in the gap-filling literature: for each basin the reconstruction is repeated with the surface observations of a station on the far side of an orographic barrier, at a distance where a purely regional signal would still be shared. A method that merely exploits regional covariance should be largely indifferent to this substitution; one that recovers basin-specific dynamics should degrade under it. The control therefore tests the central claim rather than illustrating it.

Study areas and data

The two basins share a ventilation mechanism but differ in the geometry that produces it. Sofia occupies a small, almost fully enclosed depression at approximately 550 m elevation, ringed on three sides by massifs rising 1 000–2 300 m above the valley floor. The Po Valley is an order of magnitude larger in area but is closed on its northern and southern margins by the Alps and the Apennines, and drains only eastward to the Adriatic. The practical difference is the length scale over which an air mass can be exchanged: Sofia's basin is small enough that a single inversion seals the whole urban area, whereas Po Valley episodes develop as a regional-scale pool (Fig. 1).

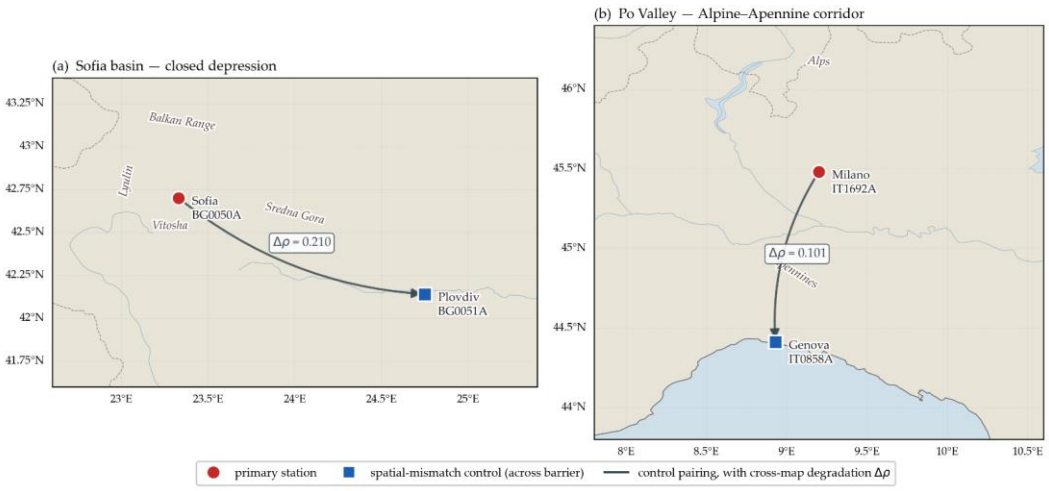


Fig. 1. Topographic setting of the two stagnation basins and the geometry of the spatial-mismatch controls. (a) The Sofia basin, a closed depression bounded by Vitosha to the south, the Balkan Range to the north and Lyulin to the west; the control station Plovdiv (BG0051A) lies 130 km east-southeast across the Sredna Gora ridge, in a separate sub-basin of the Thracian plain. (b) The western Po Valley, bounded by the Alps to the north and the Apennines to the south; the control station Genova (IT0858A) lies 120 km south across the Apennine watershed on the Ligurian coast. Circles mark primary stations, squares mark controls; arrows indicate the control pairing and are annotated with the measured degradation in cross-map correlation (Δρ) when the control station's surface observations are substituted for the native ones. Elevation from [DEM source, resolution]; station coordinates from the EEA Air Quality e-Reporting database [14].

Each basin is paired with a negative-control station chosen to sit across an orographic barrier at a distance where a purely regional signal would still be shared. Plovdiv (BG0051A) lies 130 km east-southeast of Sofia, separated by the Sredna Gora ridge, in a different sub-basin of the Thracian plain. Genova (IT0858A) lies 120 km south of Milano, separated by the Apennine watershed, and is coastal rather than continental. If the reconstructed dynamics were regional, the control pairing would perform comparably to the native pairing.

Table 1. Characteristics of the two basin stations and their spatial-mismatch controls. Both primary stations are EEA urban-background sites; both controls lie across an orographic divide from their paired basin at comparable great-circle distance. Basin elevation refers to the valley floor at the station. The canonical configuration denotes the embedding variant selected by out-of-sample prediction skill in the source study [11] and is held fixed throughout the present analysis; A4V admits boundary-layer height as an explicit embedding coordinate, A3 uses the full multivariate embedding without it.

	Sofia	Milano
Station code	BG0050A	IT1692A
Station type	urban background	urban background
Basin elevation	~550 m	~120 m
Confinement	closed depression, 3 sides	valley, N and S margins
Dominant winter source	solid-fuel heating + traffic	traffic + industry
Control station	Plovdiv (BG0051A)	Genova (IT0858A)
Barrier	Sredna Gora ridge	Apennine watershed
Control distance	~130 km	~120 km
Canonical configuration	A4V (PBLH in-view)	A3 (full multivariate)

Satellite data are TROPOMI/Sentinel-5P tropospheric NO_2 vertical column densities, processor version 2.4 and later, for 2019–2024, screened at qa_value > 0.75 [12, 13]. Columns are reported in µmol m^{-2}. For each station the nearest valid pixel centroid within 10 km is selected per overpass; median colocation distance is 2.3–2.6 km, smaller than the nadir pixel footprint of approximately 5.5 × 3.5 km. Surface NO_2 and O_3 come from the EEA Air Quality e-Reporting database for the same stations [14]. Boundary-layer height, 10 m wind components and solar zenith angle are taken from ERA5 reanalysis [15].

Method

The reconstruction framework is described in full in [11]; this section states only what is needed to read the results.

Urban NO_2 is treated as a forced, non-autonomous nonlinear dynamical system. Rather than fitting a regression from covariates to the missing column, the method reconstructs a shadow manifold of the system's state space from observed variables and fills gaps by navigating to dynamical analogues on that manifold. The theoretical basis is Takens' embedding theorem [16] in the multivariate form of Deyle and Sugihara [17], extended to forced systems by Stark [18]: a system driven by an external forcing remains reconstructible provided the forcing variables are themselves admitted as embedding coordinates. This is why boundary-layer height and solar zenith angle enter as explicit coordinates rather than as regression features – they keep analogues within a common photochemical and mixing regime.

Multivariate state-space reconstruction (MSSR) generates candidate embeddings from surface NO_2, surface O_3, boundary-layer height, wind components and solar zenith angle, and retains the highest-skill views by Simplex prediction [19]. Gap values are inferred as an exponentially weighted average over $k = 10$ nearest neighbours on the retained manifolds, with the clear-sky sampling bias corrected by stabilised inverse probability weighting folded into the analogue weights, so that the scarce cloudy-stagnant analogues present in the library are up-weighted in proportion to their inverse selection probability. Convergent cross mapping [20] acts as an operational validity gate: where the surface sensor and the satellite column fail to show convergent coupling, the gap is flagged out-of-manifold and left unfilled rather than imputed.

Two fidelity metrics are used alongside RMSE and correlation. The Manifold Overlap Ratio in its extreme-subset form (MOR_ext) measures the fraction of recurrent pairs in the observed extreme subset that are also recurrent in the predicted trajectory, at recurrence threshold ε set to the 10th percentile of pairwise distances – within the 5–15% range recommended for recurrence analysis [21] – embedding dimension $E = 3$ and extreme quantile $q = 0.95$. Dynamic Trend Capture (DTC) measures agreement in the sign of successive increments. Both are geometric rather than pointwise: a method that minimises RMSE by flattening peaks scores well on RMSE and poorly on MOR_ext, which is the behaviour the metrics are designed to expose. MOR_ext and DTC are therefore not alternative accuracy scores but a different question asked of the same prediction. RMSE asks how far the reconstructed values lie from the observations; MOR_ext and DTC ask whether the reconstructed trajectory visits the same region of state space and moves in the same direction. A reconstruction can be close in the first sense while being wrong in the second, and for episode detection it is the second that decides whether the output is usable

Baselines are Random Forest in two configurations, climatology, persistence and linear interpolation. The fair-comparison Random Forest (RF_METEO) is denied surface NO_2, so that its disadvantage cannot be attributed to information asymmetry; it uses 500 trees, maximum depth 15 and minimum leaf size 5.

Results

The winter inversion regime is a distinct region of state space

In both basins the reconstructed state space separates into two populated regions corresponding to the two ventilation regimes. The winter corner is characterised by low boundary-layer height, high surface NO_2 and suppressed O_3; the summer corner by deep mixing, low NO_2 and high photochemical O_3. Colouring the library points by observed TROPOMI column shows that the highest columns are not scattered through the state space but concentrate in the low-PBLH, high-NO_2 corner (Fig. 2).

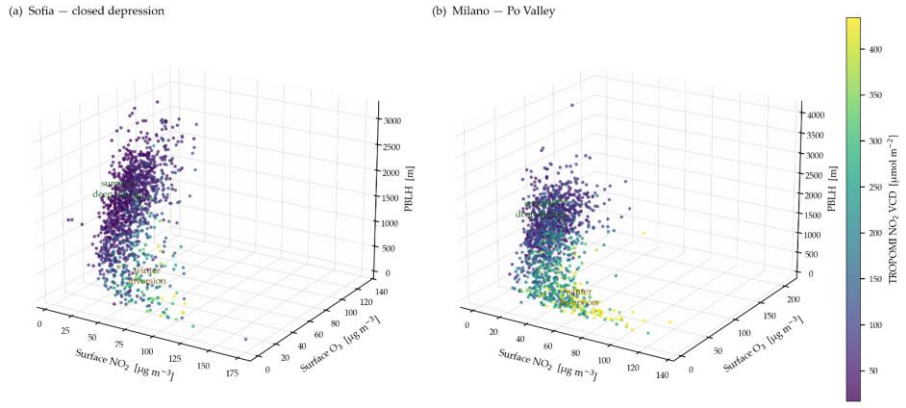


Fig. 2. Reconstructed state space at the two basin stations, 2019–2024. Each point is one TROPOMI overpass placed by its coincident surface NO_2, surface O_3 and ERA5 boundary-layer height, and coloured by the observed tropospheric NO_2 column. (a) Sofia (BG0050A), N = 1325 overpasses. (b) Milano (IT1692A), N = 1382. Both basins separate into two populated regions: a winter corner at low boundary-layer height, elevated surface NO_2 and suppressed O_3, where the highest columns concentrate, and a summer corner at deep mixing, low NO_2 and high photochemical O_3. The separation is more compact at Sofia. Overpasses lacking any of the three embedding coordinates are excluded, which accounts for the difference between N here and the total paired record. Colour scale shared between panels; VCD in µmol m⁻².

The separation is more compact at Sofia than at Milano, consistent with a smaller basin in which a single inversion seals the whole urban area rather than developing as a regional pool. Because the episodes form a regime rather than a distribution tail, analogue neighbours drawn from within that corner escape the pull toward the densely populated centre that constrains a globally fitted regressor.

Missing data concentrate where the episodes are

The MNAR structure is directly visible in the day-of-year coverage. Valid overpasses are sparse from November through February in both basins, and the same months carry the highest observed columns. The gaps are not distributed uniformly across the record; they are concentrated in precisely the interval that determines episodic exposure (Fig. 3).

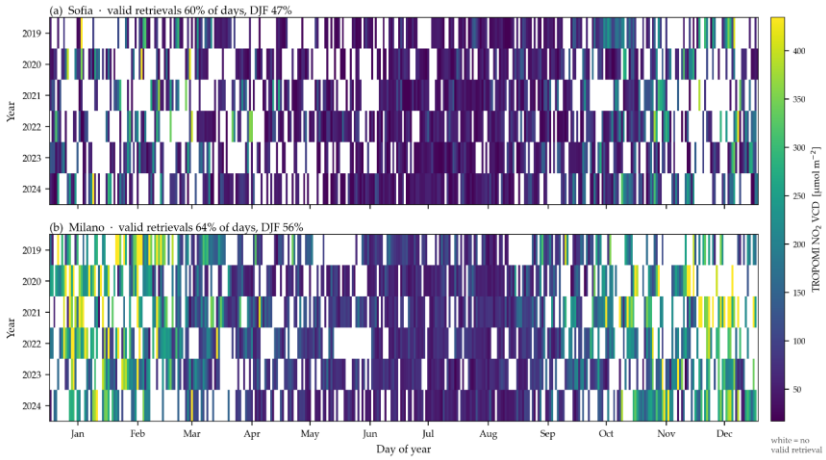


Fig. 3. Temporal structure of data loss and column magnitude, 2019–2024. Each cell is one day; colour gives the observed tropospheric NO_2 column where a quality-screened retrieval exists (qa_value > 0.75), white indicates no valid retrieval. (a) Sofia (BG0050A): valid retrievals on [X]% of days overall and [Y]% in December–February. (b) Milano (IT1692A): [X]% and [Y]% respectively. In both basins the white bands concentrate in the same winter months that carry the highest observed columns, which is the missingness structure the reconstruction framework is designed to address. Colour scale shared between panels; VCD in µmol m⁻²

Extreme episodes survive reconstruction

Milano experienced two successive Po Valley inversion episodes in autumn 2022 (Fig. 4a), with observed columns of 414 µmol m⁻² on 8 November and 405 µmol m⁻² on 7 December, both separated from the preceding valid overpass by multi-day cloud gaps. The reconstruction reproduces both episodes in amplitude and in timing. Across the 2022 holdout year the reconstruction attains r = 0.997 against the valid overpasses, with RMSE = 13 µmol m⁻². The fair-comparison Random

Forest, given the same meteorological inputs, follows the seasonal trend but underestimates every episode peak, with RMSE = 80 µmol m⁻² and r = 0.730.

Sofia shows the same qualitative behaviour at lower absolute amplitude (Fig. 4b), as expected from its smaller emission inventory, with the solid-fuel heating signature producing a sharper late-autumn onset than the Po Valley's more gradual accumulation.

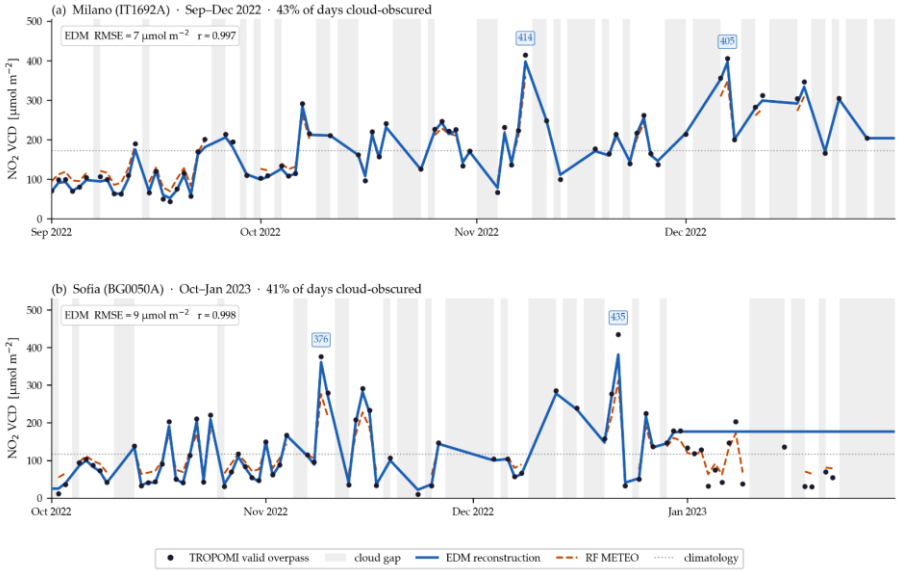


Fig. 4. Episode reconstruction during the XY_A held-out year (2022), in which no test-period observation entered the reconstruction library. (a) Milano (IT1692A), September–December 2022, spanning two Po Valley inversion episodes with observed columns of 414 and 405 µmol m⁻². (b) Sofia (BG0050A), equivalent winter window. Filled circles are quality-screened TROPOMI overpasses; grey bands mark days without a valid retrieval, across which the reconstruction (solid line) is continuous. Skill is evaluated only at valid overpasses and is annotated on each panel. The dashed RF METEO trace is not a per-overpass model output: it is reconstructed by applying the published predicted-to-observed standard-deviation ratio for that station (σ_pred/σ_obs = 0.769 at Milano, 0.610 at Sofia [11]) to the observed series, and is shown to illustrate the variance-compression behaviour those published statistics describe. The dotted line is the seasonal mean. VCD in µmol m⁻².

Variance compression separates the methods

The episode behaviour generalises across the full evaluation. Under the MCAR mask protocol, extreme-subset manifold overlap reaches MOR_ext = 0.915 at Milano and 0.618 at Sofia, while every non-EDM method - Random Forest, climatology, persistence and linear interpolation alike – returns MOR_ext = 0.000 at the per-replicate level under the canonical parameterisation; summary medians across mask replicates remain below 0.05. The separation is not a threshold artefact, and persists across variations in ε, E and q [11].

The mechanism is variance compression. RF_METEO reproduces predicted-to-observed standard deviation ratios of 0.61 at Sofia and 0.77 at Milano: the predicted trajectory is a contracted copy of the observed one, which is sufficient to place every extreme prediction inside the observed extreme threshold and therefore to drive MOR_ext to zero. The same contraction costs accuracy – RMSE rises from 9.3 to 35.5 µmol m⁻² at Sofia and from 13.0 to 80.2 µmol m⁻² at Milano – so the advantage of the reconstruction exceeds a factor of four at both stations, under conditions that favour the baseline. Fig. 5 shows this directly. At both stations the reconstructed values track the 1:1 reference across the full observed range, including the upper 15% of the distribution, while the variance-compressed baseline departs from the reference progressively as the observed column rises – the geometric signature that MOR_ext measures.

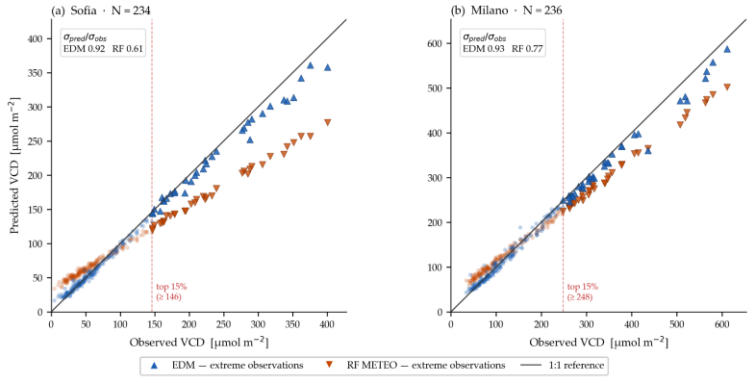


Fig. 5. Observed against predicted tropospheric NO_2 column, XY_A held-out year (2022). (a) Sofia (BG0050A), N = [N]. (b) Milano (IT1692A), N = [N]. Small markers are the full test set; triangles mark the upper 15% of observed values, above the threshold indicated by the dashed vertical line. The solid line is the 1:1 reference. Reconstructed values lie along the reference across the full range including the extreme subset; the RF METEO points fall increasingly below it as the observed column rises, which is the regression toward the conditional mean that drives MOR_ext to zero for pointwise-optimised predictors. As in Figure 4, the RF METEO values are reconstructed from the published σ_pred/σ_obs ratios for each station [11] rather than taken from per-overpass model output. Predicted-to-observed standard-deviation ratios are annotated on each panel. VCD in µmol m⁻².

The recovered dynamics are basin-specific

The spatial-mismatch control tests whether the reconstruction is exploiting a genuine station-pixel coupling or a regional signal available anywhere in the vicinity. Substituting the control station's surface observations for the native ones degrades the cross-map correlation by Δρ = 0.210 at Sofia and Δρ = 0.101 at Milano.

The control stations were not selected on distance alone. Plovdiv and Genova each lie across a topographic divide from their paired basin – the Sredna Gora ridge and the Apennine watershed respectively – so that the substitution breaks the shared ventilation regime while preserving synoptic-scale proximity. This separates the two hypotheses cleanly: regional covariance survives the barrier, basin-specific dynamics do not.

Both degradations are substantial, but the Sofia value is roughly twice the Milano value. This is the expected ordering. Sofia's basin is small and fully enclosed, so the dynamical state at Plovdiv – in a separate sub-basin across the Sredna Gora ridge – carries little information about Sofia's ventilation state. The Po Valley is large enough that Milano and Genova, although separated by the Apennine watershed, share more synoptic forcing. The control result therefore does double duty: it rules out the regional-signal explanation in both basins, and the contrast between the two Δρ values is itself consistent with the topographic difference.

Discussion and conclusions

The two basins give the same answer by different routes. In both, the winter inversion regime occupies a separable region of the reconstructed state space; in both, extreme episodes survive analogue reconstruction while every pointwise-optimised baseline compresses them to the conditional mean; and in both, negative controls across orographic barriers confirm that the recovered coupling is local to the basin rather than regional.

The quantitative difference between them is informative rather than incidental. Sofia's control degradation is twice Milano's, and its state-space separation is more compact. Both follow from basin geometry: a small closed depression admits a single ventilation state that applies to the whole urban area, whereas a basin the size of the Po Valley supports internal gradients and shares more synoptic forcing with its surroundings. The method's advantage is therefore largest precisely where the topography is most confining – which is also where episodic exposure is most severe.

The control design itself warrants emphasis as a transferable element. Gap-filling studies are commonly validated by withholding observations and reporting error against them – a procedure that cannot distinguish a method which has learned the local dynamics from one which has learned a regional climatology shared by every station in the vicinity. Substituting a donor station across a known physical divide costs nothing in additional data and converts that assumption into a testable prediction. It is applicable irrespective of the reconstruction method employed.

The practical consequence concerns exposure assessment. An inversion episode that coincides with multi-day cloud cover is invisible in the screened TROPOMI record and is reproduced as an attenuated bump by conventional gap-filling. Assessments built on either input will understate peak exposure, and will do so systematically rather than randomly, because the missingness

and the attenuation share a cause. Reconstruction that preserves extreme-subset geometry changes the input to those assessments, not merely their error bars.

Three limitations bound these conclusions. The analysis is station-level: it reconstructs a column time series at a station–pixel pairing and does not produce spatially continuous fields. Surface-to-column representativeness is handled implicitly through boundary-layer height as an embedding coordinate, and where the vertical profile departs strongly from the library the out-of-manifold flag diagnoses the mismatch without correcting it. Results are conditional on TROPOMI processor version 2.4 and later; sensitivity to retrieval version is not assessed here.

The framing adopted here – the basin as the unit of analysis rather than the algorithm – is deliberate. Reconstruction skill is not a property of a method in isolation; it is a property of a method applied to a system with a particular dynamical structure, and in these cases that structure is set by topography. A single headline skill figure averaged across heterogeneous sites obscures precisely the dependence that determines where the method is worth deploying. The two basins examined here differ in their confinement and differ correspondingly in their results, and it is that correspondence, rather than either result taken alone, which carries the argument.

Two basins, two topographies, one result: in enclosed stagnation basins, where cloud-driven data loss and pollution episodes share a synoptic cause, the extreme episodes that matter for exposure can be recovered – but only by a method whose objective is the geometry of the trajectory rather than the magnitude of its pointwise error.

References:

1. Van Geffen, J.; Eskes, H.; Compernolle, S.; Pinardi, G.; Verhoelst, T.; Lambert, J.-C.; Sneep, M.; ter Linden, M.; Ludewig, A.; Boersma, K.F.; Veefkind, J.P. Sentinel-5P TROPOMI NO_2 retrieval: impact of version v2.2 improvements and comparisons with OMI and ground-based data. Atmos. Meas. Tech. 2022, 15, 2037–2060.
2. Eskes, H.J.; Eichmann, K.-U. S5P Mission Performance Centre Nitrogen Dioxide [L2__NO2___] Readme; Report S5P-MPC-KNMI-PRF-NO2; European Space Agency: Noordwijk, The Netherlands, 2024.
3. Horton, D.E.; Skinner, C.B.; Singh, D.; Diffenbaugh, N.S. Occurrence and persistence of future atmospheric stagnation events. Nat. Clim. Change 2014, 4, 698–703.
4. World Health Organization. WHO Global Air Quality Guidelines: Particulate Matter, Ozone, Nitrogen Dioxide, Sulfur Dioxide and Carbon Monoxide; WHO: Geneva, Switzerland, 2021.
5. Gerber, F.; de Jong, R.; Schaepman, M.E.; Schaepman-Strub, G.; Furrer, R. Predicting missing values in spatio-temporal remote sensing data. IEEE Trans. Geosci. Remote Sens. 2018, 56, 2841–2853.
6. Belgiu, M.; Drăguţ, L. Random forest in remote sensing: a review of applications and future directions. ISPRS J. Photogramm. Remote Sens. 2016, 114, 24–31.
7. Gadzhev, G.; Ganev, K.; Miloshev, N.; Syrakov, D.; Prodanova, M. Numerical study of the atmospheric composition in Bulgaria. Comput. Math. Appl. 2013, 65(3), 402–422.
8. European Environment Agency. Europe's Air Quality Status 2024; EEA Briefing; European Environment Agency: Copenhagen, Denmark, 2024.
9. Cersosimo, A.; Serio, C.; Masiello, G. TROPOMI NO_2 tropospheric column data: regridding to 1 km grid-resolution and assessment of their consistency with in situ surface observations. Remote Sens. 2020, 12, 2212.
10. Bigi, A.; Ghermandi, G. Long-term trend and variability of atmospheric PM10 concentration in the Po Valley. Atmos. Chem. Phys. 2014, 14, 4895–4907.
11. Trenchev, P.; Avetisyan, D.; Dimitrova, M.; Trencheva, E. Station-level gap filling of TROPOMI NO_2 via physics-informed shadow manifold reconstruction. Remote Sens. 2026, 18(14), 2387. https://doi.org/10.3390/rs18142387
12. van Geffen, J.H.G.M.; Eskes, H.J.; Boersma, K.F.; Veefkind, J.P. TROPOMI ATBD of the Total and Tropospheric NO_2 Data Products; Report S5P-KNMI-L2-0005-RP, version 2.4.0; Royal Netherlands Meteorological Institute: De Bilt, The Netherlands, 2022.
13. Veefkind, J.P.; Aben, I.; McMullan, K.; Förster, H.; de Vries, J.; Otter, G.; Claas, J.; Eskes, H.J.; de Haan, J.F.; Kleipool, Q.; et al. TROPOMI on the ESA Sentinel-5 Precursor: a GMES mission for global observations of the atmospheric composition for climate, air quality and ozone layer applications. Remote Sens. Environ. 2012, 120, 70–83.
14. European Environment Agency. Air Quality e-Reporting Database. Available online: https://www.eea.europa.eu/en/datahub (accessed on 10 October 2026).
15. Hersbach, H.; Bell, B.; Berrisford, P.; Hirahara, S.; Horányi, A.; Muñoz-Sabater, J.; Nicolas, J.; Peubey, C.; Radu, R.; Schepers, D.; et al. The ERA5 global reanalysis. Q. J. R. Meteorol. Soc. 2020, 146, 1999–2049.
16. Takens, F. Detecting strange attractors in turbulence. In Dynamical Systems and Turbulence, Warwick 1980; Rand, D., Young, L.-S., Eds.; Lecture Notes in Mathematics, Volume 898; Springer: Berlin, Germany, 1981; pp. 366–381.
17. Deyle, E.R.; Sugihara, G. Generalized theorems for nonlinear state space reconstruction. PLoS ONE 2011, 6, e18295.
18. Stark, J. Delay embeddings for forced systems. I. Deterministic forcing. J. Nonlinear Sci. 1999, 9, 255–332.
19. Sugihara, G.; May, R.M. Nonlinear forecasting as a way of distinguishing chaos from measurement error in time series. Nature 1990, 344, 734–741.
20. Sugihara, G.; May, R.; Ye, H.; Hsieh, C.-H.; Deyle, E.; Fogarty, M.; Munch, S. Detecting causality in complex ecosystems. Science 2012, 338, 496–500.
21. Marwan, N.; Romano, M.C.; Thiel, M.; Kurths, J. Recurrence plots for the analysis of complex systems. Phys. Rep. 2007, 438, 237–329.